

# Synthesis of aluminium nanoparticles in a PP matrix during melt processing: Effect of the alkoxide organic chain

M. Oliveira <sup>a,\*</sup>, R. Nogueira <sup>b</sup>, A.V. Machado <sup>a</sup>

<sup>a</sup> IPC - Institute for Polymers and Composites/I3N, University of Minho, Campus de Azurém, 4800-058 Guimarães, Portugal

<sup>b</sup> ISAH - Institute of Sanitary Engineering and Waste Management, University of Hannover, Welfengarten 1, D-30167 Hannover, Germany

## Keywords:

Hybrid nanocomposite  
Aluminium nanoparticles  
Inorganic alkoxides  
Sol-gel process

## Abstract

The synthesis of aluminium nanoparticles in a polypropylene (PP) matrix by a sol-gel process in the melt was investigated. The study was performed using two aluminium precursors, aluminium isopropoxide and aluminium acetylacetonate, to assess the effect of the stereochemical hindrance of the precursor organic groups on reactivity. The hybrid nanocomposites were prepared in a batch mixer under constant processing conditions and characterized by several techniques. Chemical and morphological characterization proved that aluminium formed covalent bonds with polypropylene modified with maleic anhydride and the presence of aluminium nanoparticles. Moreover, TEM micrographs of both nanocomposites synthesised revealed a lower amount of nanoparticles when aluminium acetylacetonate was used. The values of the activation energy determined explained the higher reactivity of aluminium isopropoxide. The reaction mechanisms were proposed for both precursors.

# Introduction

Polymer nanocomposites are a new class of materials, in which at least one of the components has dimensions at the nanometric scale. These materials have drawn considerable attention, in recent years, due to the significant improvements in several properties, such as, thermal stability, flame retardancy, dielectrical properties, heat distortion temperature, barrier properties and thermal expansion coefficient [1-4]. This remarkable change of the physical and mechanical macroscopic properties can be achieved by the addition of inorganic solid nanoparticles (typically in form of fibres, flakes, spheres or fine particles) with huge surface area, which increases the interaction with the polymer.

Even though a lot of research has been done on the preparation of these materials [3-5], the homogeneous dispersion of the nanoparticles in polymeric matrices, especially in non-polar, still a difficult task. In most cases the van der Waals attraction between nanoparticles promotes the formation of clusters and agglomerates. In addition, hydrophilic nanoparticles and hydrophobic polymers are not compatible in nature, which results in poor interfacial bonding and therefore bad dispersion. Thus, frequently nanocomposites exhibited worst properties than conventional polymers, which limits their effective application [6-8]. Therefore, further

research is necessary to improve nanoparticles/polymer interaction and to develop materials with higher performance.

Three principal approaches have been used to disperse nanoparticles in a polymeric matrix: solution dispersion, melting dispersion and in situ nanoparticles formation by a sol-gel process. Solution dispersion is a direct route, which is a convenient way to study and understand, at laboratory scale, the interaction between polymer and inorganic nanoparticles. Even though, it is a simple process, it can not be used at industrial scale due to solvent elimination. Melt dispersion seems to be the most suitable and environmental friendly, as well as is solvent free method and it is compatible with current industrial process likes extrusion or injection moulding. Nevertheless, due to poor compatibility between polymeric matrices and nanoparticles, mainly with nonpolar matrices, agglomerates are often obtained. A way to improve the dispersion is by using an in situ sol-gel method, which is based on a reaction between a precursor, containing the inorganic particle, and a polymer, followed by hydrolysis-condensation reaction. In classic sol-gel reaction, hydrolysis-condensation step is performed under acid or basic conditions in solution, which is not appropriated for industrial processes [2,9,10]. Consequently, the use of this type of reactions in the melt became a challenge.

The use of a sol-gel method to prepare nanocomposites of polypropylene (PP) and metal oxides is described in the literature for a few systems [2,11,12]. The most common system studied is PP/silica nanocomposite using different silica precursors [13-16]. For example, Dou et al. prepared a PP/silica nanocomposite by solvent free sol-gel reaction, using a pre-prepared polymer, hyperbranched polyethoxysilane (PEOS) [2]. More recently, Bahloul and co-workers developed PP/TiO<sub>2</sub> nanocomposites by reactive extrusion, where titanium n-butoxide (Ti(OR)<sub>4</sub>) was used as precursor [17].

Therefore, the present work aims to prepare well dispersed aluminium nanoparticles in a PP matrix using a sol-gel process in the melt. Since PP does not have reactive groups to form covalent bonds with the precursor, PP modified with maleic anhydride (PP-g-MA)

was used. Moreover, two precursors with different organic chain, aluminium isopropoxide ( $\text{Al}(\text{Pr} - \text{i} - \text{O})_3$ ) and aluminium acetylacetonate ( $\text{Al}(\text{acac})_3$ ), were selected to investigate the effect of the precursor organic chain in the sol-gel reaction. The hybrid nanocomposites were prepared in a batch mixer and were characterized using several analytical techniques.

## Experimental

### Materials

Polypropylene modified with maleic anhydride (PP-g-MA, Polybond 3200) with a melting temperature around  $160^\circ\text{C}$  and a MA content of 1wt.%, was supplied by Crompton. Aluminium isopropoxide ( $\text{Al}(\text{Pr} - \text{i} - \text{O})_3$ ) and aluminium acetylacetonate ( $\text{Al}(\text{acac})_3$ ), both in powder state, were used as received and were supplied by Sigma Aldrich and Acros Organics, respectively.

### Synthesis

PP containing aluminium nanoparticles was prepared in the melt, in a Haake batch mixer (Rheocord 90 ; volume 60 mL ), equipped with two rotors running in a counter-rotating way. The rotor speed was 50 rpm and the set temperature was  $180^\circ\text{C}$ . The following procedure was adopted to prepare the nanocomposites, first pellets of PP-g-MA were introduced into the hot mixer, after melting, the aluminium precursor was added in a ratio 1: 1 (maleic anhydride/precursor). The total sample was removed after 10 minutes mixing. The hybrid polymer nanocomposite (HPN) synthesized with  $\text{Al}(\text{Pr} - \text{i} - \text{O})_3$  was called *HPN - Pr* and the HPN synthesized with  $\text{Al}(\text{acac})_3$  was called *HPN-acac*.

Sheets of 1 mm thickness were prepared by compression moulding from the sample collected from the mixer. These sheets were placed in an acidic solution (HCl 1M) and the hydrolysis-condensation reaction was carried out at  $80^\circ\text{C}$  according to the Sioplast process [9].

## Structural characterization

### FT-IR

Infrared spectra of all HPNs were recorded in transmission mode between 400 and  $4000\text{ cm}^{-1}$  using a Perkin Elmer 1610, with 32 scans and resolution of  $4\text{ cm}^{-1}$ . Thin films were previously prepared by compression moulding in a hot press at  $180^\circ\text{C}$  and analyzed directly using a solid film support.

### XRD

X-ray diffraction (XRD) spectra of the samples were obtained at room temperature using a Bruker D8 Discover X-ray equipment with Ni-filter. The applied current and accelerating voltage were 40 mA and 40 kV , respectively.

### XPS

X-ray Photoelectron Spectroscopy (XPS) was performed using a Thermo Scientific K-Alpha ESCA instrument equipped with aluminium Ka 1.2 monochromatized radiation at 1486.6 eV X-ray source. Due to the insulating nature of the samples it was necessary to use an electron flood gun in order to minimize surface charging. Neutralization of the surface charge was achieved using both a low energy flood gun, in the range of 0 – 14eV, and a low energy Argon ions gun. The XPS measurements were carried out using monochromatic Al-K  $\alpha$  radiation ( $h\nu = 1486.6\text{eV}$ ). Photoelectrons were collected from a 90° take-off angle relative to the sample surface. The measurement was done in the Constant Analyser Energy mode (CAE) with 100 eV pass energy for survey spectra and 20 eV pass energy for high-resolution spectra. Charge reference was done by setting the lower binding energy C1s peak at 285.0 eV for the C1s hydrocarbon peak.

## **SEM and EDS**

Scanning electron microscopy (SEM) analysis was performed in a Leica Cambridge S360 microscope. The samples were previously fractured in liquid nitrogen and coated with a gold thin film. X-ray microanalysis mapping was performed with an energy dispersive X-ray Spectrometer (EDS) from Link eXL II from Oxford Instruments attached to the SEM.

## **TEM**

Samples of 100 nm thickness were cut using a diamond knife, in a Leica ultramicrotome at  $-140^{\circ}\text{C}$ . The cut sections were transferred onto copper grids and then analysed in a Philips CM120 transmission electron microscope (TEM).

## **Rheological properties**

The rheological behaviour of the initial polymer and prepared HPNs was determined by oscillatory rheological measurements carried out in a Paar Physica MCR300 rheometer at  $180^{\circ}\text{C}$ . The gap and diameter of the plates was 1 mm and 25 mm, respectively. A frequency sweep from 0.1 Hz to 100 Hz under constant strain in the linear viscoelastic region was performed for each sample. Nitrogen atmosphere was used to prevent thermo-oxidative degradation.

## **Gel content**

Around 150 mg of the HPNs were used to determine the gel content. HPNs previously weighted were placed in a 125 -mesh stainless steel basket. All cages were weighted and then immersed in hot xylene at  $140^{\circ}\text{C}$  until weight equilibrium. The final weight was determined after drying the samples in a vacuum oven at  $105^{\circ}\text{C}$  during the night. The gel content was calculated as the weight of non-extractable material divided by the total weight of the original sample and was expressed as the percentage.

## **TGA and DSC**

Thermogravimetric measurements for all HPNs were carried out using a TA Q500 thermobalance. Samples were heated from  $30^{\circ}\text{C}$  to  $600^{\circ}\text{C}$  at  $10^{\circ}\text{C}/\text{min}$  under a nitrogen flow ( $50\text{ mL}/\text{min}$ ).

Thermal properties of HPNs were measured using a Perkin Elmer Diamond DSC 131 apparatus, equipped with an LNCS (Liquid Nitrogen Cooling System) accessory. Samples (about 10 mg) are placed in Al pans and heated at  $10^{\circ}\text{C}/\text{min}$  from  $30^{\circ}\text{C}$  to  $220^{\circ}\text{C}$  under

nitrogen flow. The crystallinity degree ( $X_c$ ) was calculated by the ratio of  $\Delta H_f$  (the apparent melt enthalpy calculated from DSC curves as the melting enthalpy per gram) of the component and  $\Delta H_f^0$  (the theoretically melt enthalpy component in its completely crystalline state).

## Activation energy

The activation energy ( $E_a$ ) of the HPNs synthesized using the two inorganic precursors was determined using gel content values. For each precursor the HPNs were prepared at three different temperatures (170, 180 and 200°C) according to the procedure described above and samples were collected after 0.5, 2 and 5 min of mixing. For all the samples, the gel content was measured as according to the method described previously. For each temperature, the crosslinking rate was determined as the slope of gel content *vs* time reaction, as described by Shieh [18]. Then, the  $E_a$  was calculated from the plot of the crosslinking reaction rate at the three different temperatures as a function of the reciprocal absolute temperature, according to the Arrhenius equation:

$$\ln(k) = \ln A - \frac{E_a}{R} \frac{1}{T} \quad (1)$$

where  $k$  is the crosslinking rate,  $E_a$  is the activation energy,  $R$  is the gas constant, and  $T$  is the absolute temperature.

# Results and discussion

## Structural characterisation

The FT-IR spectra of PP-g-MA, HPN-Pr and HPN-acac are presented in Fig. 1. Analysing the FT-IR spectra, there are two spectral ranges that are important to take into consideration, one between 3000 – 3500  $\text{cm}^{-1}$  and the other 400 – 1000  $\text{cm}^{-1}$ , where the OH and Al – O stretching modes occur, respectively. In HPN-Pr spectrum, depicted in Fig. 1a, a very broad band appears around 3450  $\text{cm}^{-1}$ , this band corresponds to the stretching mode of Al – OH, which is confirmed by the respective bending mode band at 1627  $\text{cm}^{-1}$  with medium intensity.

In the HPNs structure, aluminium can exist in two different coordination states, octahedral and tetrahedral [19,20]. While a broad band of stretching mode between 500 and 750  $\text{cm}^{-1}$  confirms the tetrahedral coordination, the stretching mode band in the region of 640-500  $\text{cm}^{-1}$  evidences the octahedral coordination. However, giving the broad bands in the HPN-Pr spectrum, the tetrahedral Al-O coordination seems to prevail.

The spectrum of HPN-acac sample collected from the mixer (Fig. 1b) does not show any evidence of Al – O formation. Moreover, two bands at 1520  $\text{cm}^{-1}$  and 1580  $\text{cm}^{-1}$  characteristics of acetylacetonate (acac) group, which should come out during the synthesis as secondary reaction product, still present. This means that the hydrolysis reaction did not take place in the mixer. This could be associated to the difference between  $\text{Al}(\text{acac})_3$  melting temperature (190°C) and the set temperature (180°C). Since the melt temperature increased during mixing and a constant value of 193°C was reached after 5 min, the precursor was sufficiently melted to react with the polymer. Therefore, to

overcome the low reactivity, HPN-acac was subject to a hydrolysis treatment during 96 h to

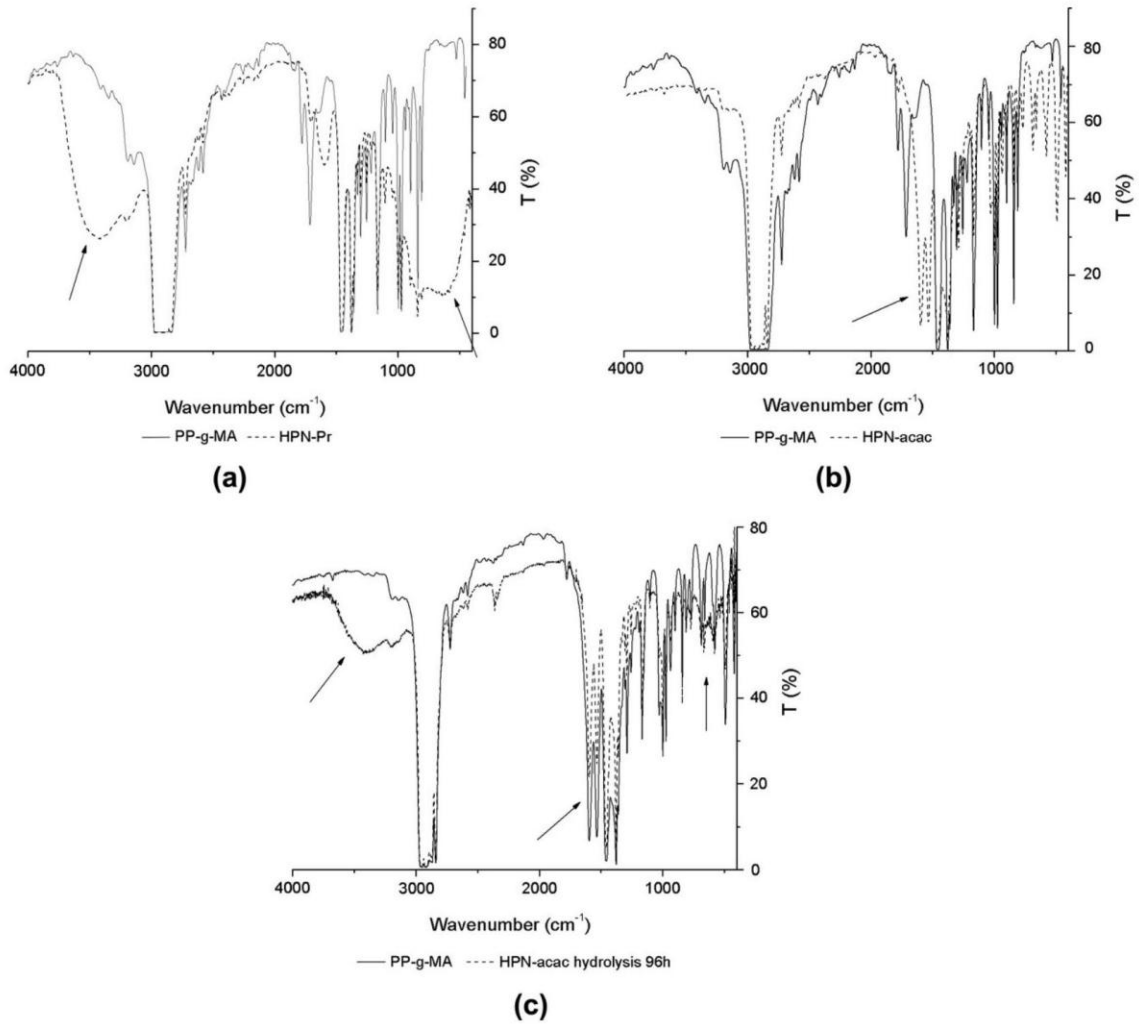


Fig. 1. - FT-IR spectra of a) PP-g-MA and HPN-Pr; b) PP-g-MA and HPN-acac and c) HPN-acac before and after hydrolysis.

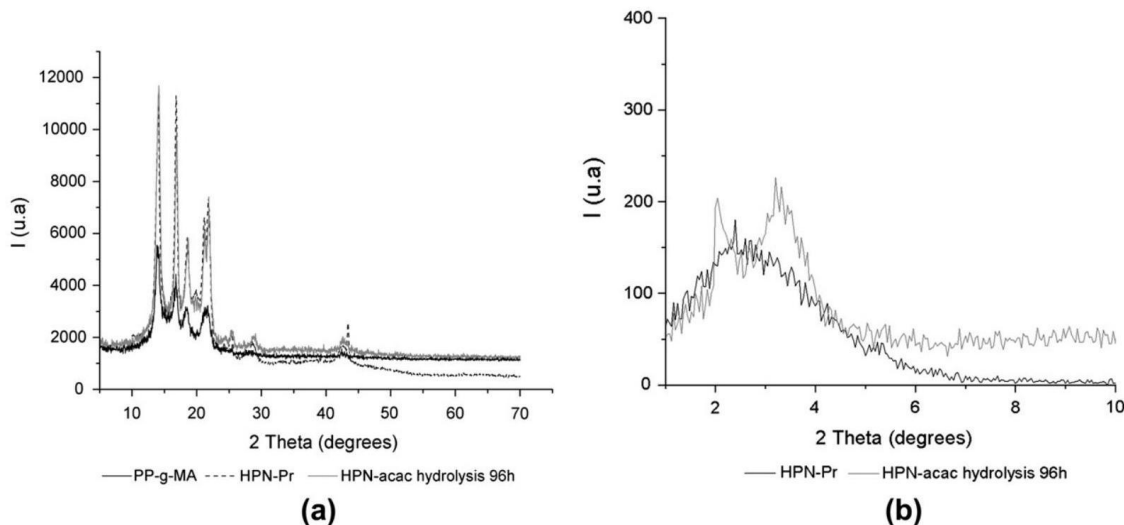


Fig. 2. - XRD pattern for a) PP-g-MA, HPN-Pr and HPN-acac after hydrolysis and b) HPN-Pr and HPN-acac after hydrolysis for low angles. promote the reaction between  $\text{Al}(\text{acac})_3$  and MA group of PP-g-MA. The spectrum recorded after this treatment (Fig. 1c) shows a decrease of the acac bands and the appearance of the Al-OH band between  $3000$  and  $3500 \text{ cm}^{-1}$ . However, in the range of  $400 - 1000 \text{ cm}^{-1}$ , where the stretching mode of Al-O occurs, no significant peak can be detected.

The XRD spectra of PP-g-MA, HPN-Pr and HPN-acac are shown in Fig. 2. The crystalline peaks at  $14^\circ$ ,  $16.8^\circ$ ,  $18.4^\circ$  and  $21^\circ$  in XRD pattern corresponding to (110), (040), (130) and (041) planes, respectively, confirm the monoclinic form of the PP-g-MA [21].

The comparison of the PP-g-MA and HPN-Pr spectra reveals new peaks at  $19.8^\circ$ ,  $20.9^\circ$ ,  $23.9^\circ$ , and  $44.23^\circ$  (Fig. 2a). The new peaks might be due to the presence of aluminium oxide hydroxide ( $\text{AlOOH}$ ) and aluminium hydroxide ( $\text{Al}(\text{OH})_3$ ), as observed by FT-IR. As indicated by Ervin and Osborn, the formation of aluminium oxy-hydroxide phase is thermodynamic favoured in a temperature range of  $130 - 350^\circ\text{C}$  [22]. However, the total number of peaks characteristics of either  $\text{AlOOH}$  or  $\text{Al}(\text{OH})_3$  are not present in the spectra or are hindered by others more intense, which makes difficult to conclude if these two species are really present [23-25].

Contrarily to HPN-Pr XRD result, HPN-acac after 96 h hydrolysis shows less peaks corresponding to aluminium oxide formation, which is in agreement with previous FT-IR analysis.

The comparison the HPN-Pr and HPN-acac after hydrolysis patterns at low angles (Fig. 2b) reveals a shift between the peaks of the two nanocomposites. While the peak of the HPN-Pr is at  $2.2^\circ$ , the peak of HPN-acac is at  $3.2^\circ$ . This can be an indication that the aluminium nanoparticles are better dispersed in the PP-g-MA matrix in HPN-Pr. Similar observation was made by Wu in the study of  $\text{PCL}/\text{TiO}_2$  and  $\text{PCL-g-AA}/\text{TiO}_2$  composites [26]. He observed two peaks at  $2.9^\circ$  and  $2.6^\circ$  for  $\text{PCL}/\text{TiO}_2$  and  $\text{PCL-g-AA}/\text{TiO}_2$ , respectively.

The peak at low angle was associated to a well and homogeneous dispersion of  $\text{TiO}_2$  in the PCL matrix.

The X-ray photoelectron spectroscopy analysis (XPS) was performed only for HPN-Pr and the values of binding energies and areas for all peaks are summarized in Table 1. The Al 2p peak of the aluminium isopropoxide ( $\text{Al}(\text{Pr}-i-\text{O})_3$ ) appears at 74.477 eV and it was shifted to 75.075 eV in the HPN-Pr. According to the literature, the binding energy of Al 2p for  $\text{Al}_2\text{O}_3$  appears in the range of 74.4-75.8 eV (27). The shift observed for Al 2p signal can be due to a complex formation ( $-\text{C}(=\text{O})-\text{O}-\text{Al}-$ ) between PP-g-MA and  $\text{Al}(\text{Pr}-i-\text{O})_3$ , which changed the aluminium neighbour groups and therefore its binding energy.

For O 1s peak of  $\text{Al}(\text{Pr}-i-\text{O})_3$  and HPN-Pr a large peak can be observed between 527 and 538 eV, respectively. After peak deconvolution two oxygen species (531.462 and 532.590 eV) can be detected (Table 1). In general, peaks around  $\approx 530$  eV are attributed to oxides ( $\text{O}_o$ ) whereas peaks around  $\approx 532$  eV are considered to adsorbed oxygen ( $\text{O}_a$ ) [21]. The  $\text{O}_a$  with higher binding energy corresponds to strongly adsorbed oxygen as -OH or  $\text{H}_2\text{O}$ . The O 1s peak of HPN-Pr has similar binding energy to  $\text{Al}(\text{Pr}-i-\text{O})_3$ . Although crosslinking took place, the sol-gel reaction did not change significantly the oxygen atoms neighbourhood.

The O/Al atomic ratio of the HPN-Pr is much lower than for the precursor. This value is related with the hydroxyl fraction present in the HPN-Pr and gives information on the oxidation evolution [27,28]. Brand and co-workers indicated in their study that for a completely anhydrous amorphous oxide layer ( $\text{Al}_2\text{O}_3$  with a hydroxyl fraction of zero) the value of the O/Al atomic ratio corresponds to 1.5, while for crystalline  $\text{AlOOH}$  (with a hydroxyl fraction of 0.5) the ratio is 2.0 [29]. The atomic ratio obtained for HPN-Pr was 1.8, which is in agreement with the FT-IR and XRD results and confirms that  $\text{AlOOH}$  groups are presented in nanocomposite prepared.

Table 1 XPS peaks values obtained for  $\text{Al}(\text{Pr}-i-\text{O})_3$  and HPN-Pr. 1

	Al 2p		O 1s				Atomic ratio $\text{O}_o/\text{Al}$
			$\text{O}_o$		$\text{O}_a$		
	Binding energy (eV)	Area	Binding energy (eV)	Area	Binding energy (eV)	Area	
$\text{Al}(\text{Pr}-i-\text{O})_3$	74.477	37478.3	531.137	158472.6	532.250	244428.8	4.034
HPN-Pr	75.075	5158.9	531.462	10630.6	532.590	16500.6	1.808

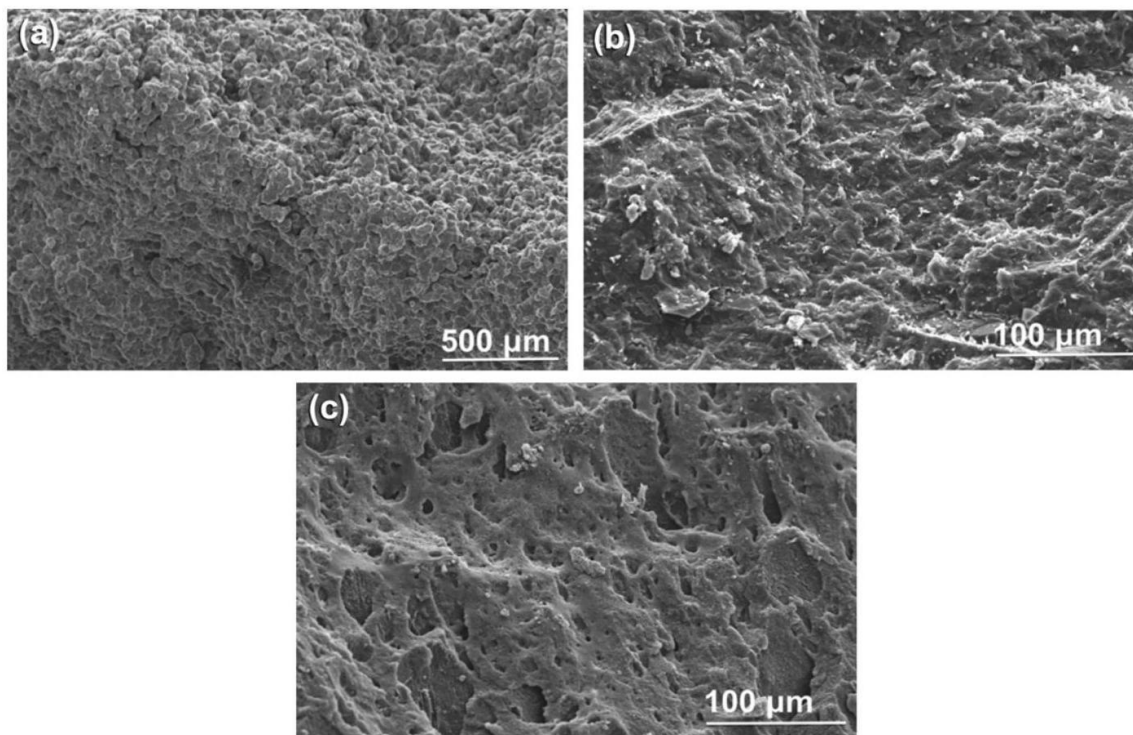


Fig. 3. SEM micrographs of a) HPN-Pr surface, b) HPN-acac surface and c) HPN-acac surface after hydrolysis treatment.

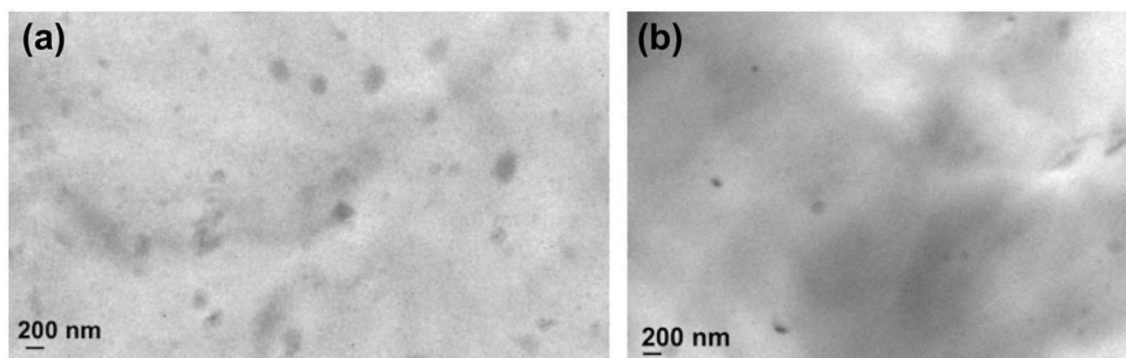


Fig. 4. TEM micrographs of a) HPN-Pr and b) HPN-acac.

Microscopic techniques were used to characterize the morphology of HPNs as well as its chemical composition. SEM micrographs presented in Fig. 3a shows that HPN-Pr has a homogeneous and rough surface. The presence of aluminium agglomerates can not be observed in the micrographs, which indicates a good dispersion and interaction between organic and inorganic components. Fig. 3b and c depict the surface morphology for HPN-acac before and after hydrolysis, respectively. Comparing the surface of HPN-acac and HPN-Pr, it is clear that the former is smoother. The hydrolysis treatment of HPN-acac provokes a strong change on the surface morphology, the presence of holes can be observed in Fig. 3c. These holes can be due to the lost of  $\text{Al}(\text{acac})_3$  particles during the hydrolysis treatment, as it will be explained below.

Since agglomerates were not observed by SEM analysis and in order to have more detail on particle size and its distribution, the samples were analysed by TEM and the results are presented in Fig. 4. The morphology of HPN-Pr (Fig. 4a) evidence well dispersed aluminium nanoparticles ( $\pm 200$  nm) in the PP matrix. Even though a good dispersion is observed for HPN-acac (Fig. 4b), the number of aluminium nanoparticles is lower than for HPN-Pr. In agreement with the previous results, this difference can be explained by the lower extension of the chemical reaction.

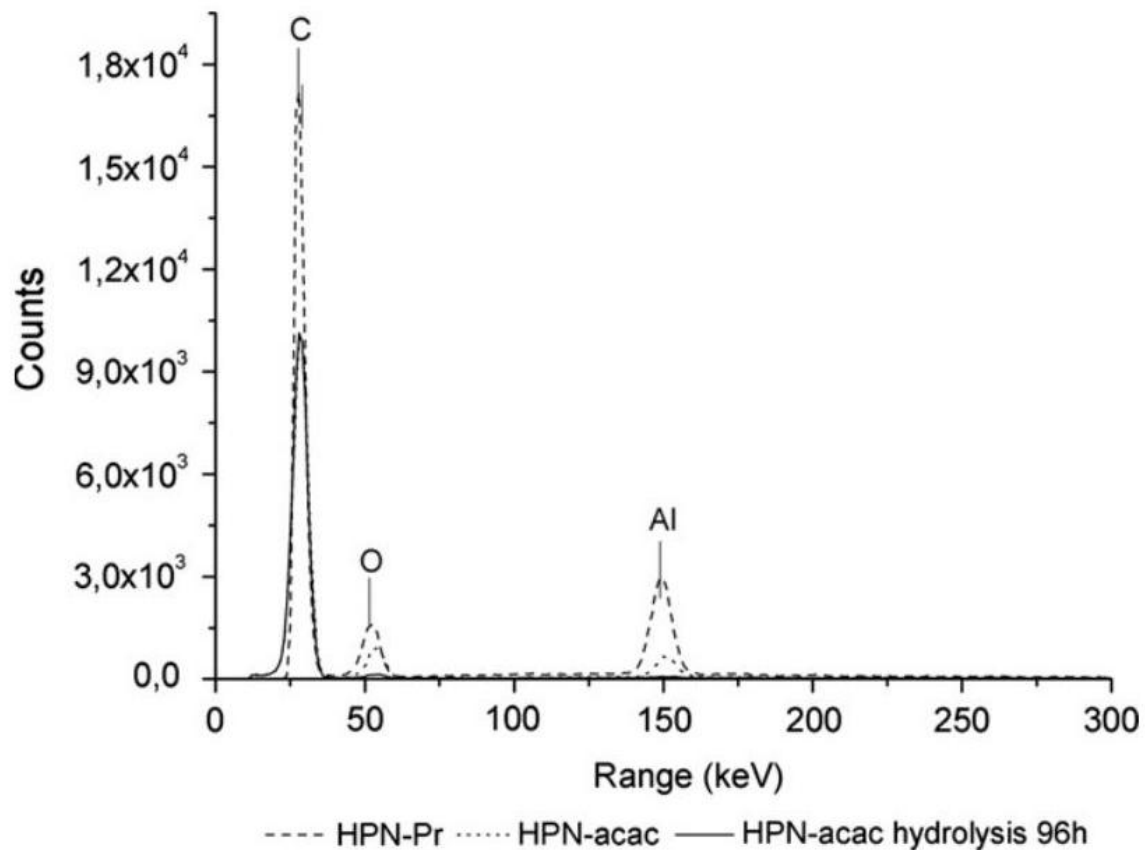


Fig. 5. - EDS spectrum of HPN-Pr and HPN-acac.

Fig. 5 shows the EDS analysis performed on the HPNs surfaces. The presence of aluminium is confirmed for both materials. However, a clear decrease of the aluminium peak intensity was

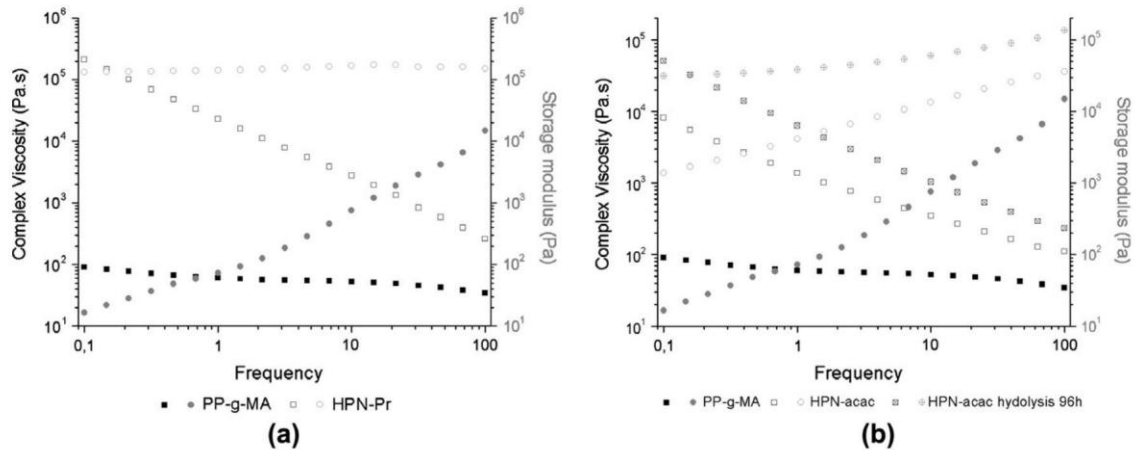


Fig. 6. - Rheological behaviour of a) PP-g-MA and HPN-Pr and b) PP-g-MA and HPN-acac before and after hydrolysis. This can explain the holes observed by SEM, part of the  $Al(acac)_3$  was lost during hydrolysis treatment from PP-g-MA matrix. In order to confirm this, both HPNs were immersed in acidic water solution during 5 days, then the aluminium concentration in the solution was analysed by atomic absorption. The results revealed that  $6.9 \times 10^{-3} \pm 1.9 \times 10^{-3} \text{ mg/L}$  and  $5.5 \pm 0.4 \text{ mg/L}$  of Al were presented in the solution of the HPN-Pr and HPN-acac, respectively.

The rheological behaviour of the prepared HPN gives important information about its molecular structure. The results presented in Fig. 6a shows a significant difference between the viscoelastic behaviour of HPN-Pr and PP-g-MA. A strong increase in complex viscosity and storage modulus can be observed for HPN-Pr. This change can be associated with a transition from a liquid-like behaviour to a solid-like behaviour, where the storage modulus is independent of the frequency value. This type of behaviour is characteristic of the crosslinking materials, which unlike the linear ones do not show a plateau at low frequencies in complex viscosity and have in the limit a slope of -1 (solid materials). The slope of the complex viscosity of the HPN-Pr is -0.95, which evidences that HPN-Pr has a crosslinking structure. The value of the gel content obtained ( 70wt. % ) corroborates the rheological data. The rheological behaviour of HPN-acac before and after hydrolysis is depicted in

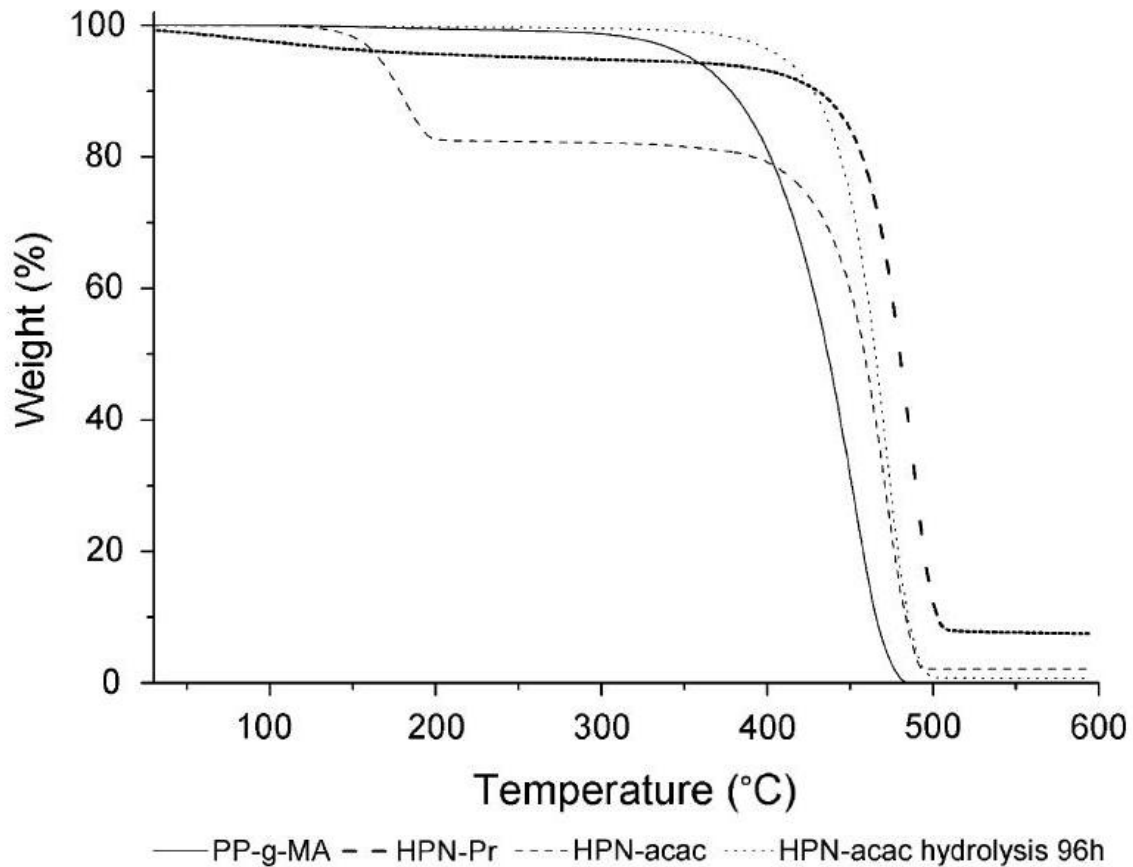


Fig. 7. - Evaluation of thermal properties of PP-g-MA, HPN-Pr and HPN-acac.

Fig. 6b. Although FT-IR and XRD results did not show any evidence that the reaction took place in the mixer, an increase in complex viscosity and storage modulus can be observed for the samples before hydrolysis. The increase in viscosity and storage modulus can not be only explained by the presence of inorganic filler in the PP-g-MA matrix but also by the formation of a branched/crosslinking molecular structure. As expected, the hydrolysis treatment promotes the reaction and the values of viscosity and storage modulus increase. The slope of complex viscosity curves increases from -0.5 to -0.75. The values of the gel content before (31.4wt%) and after hydrolysis (37.6wt.%) are in line with the rheological results. A power law relationship (Eq. (2)) can be used to analyse qualitatively the effect of hydrolysis treatment on the crosslinking degree:

$$n^* = p|w|^{a-1} \quad (2)$$

where  $n^*$  is the complex viscosity,  $w$  the angular frequency and  $P$  and  $a$  the fitting parameters. The parameter  $a-1$  corresponds to the slope of the curve  $\log(n^*)$  vs  $\log(w)$ , which reflects the shear thinning behaviour. Decrease on a value represents an increase of crosslinking. The  $a$  values obtained from Eq. (2) for HPN-acac before and after hydrolysis were 0.38 and 0.22, respectively. Fig. 8 shows the change of thermal behaviour determined by thermogravimetric

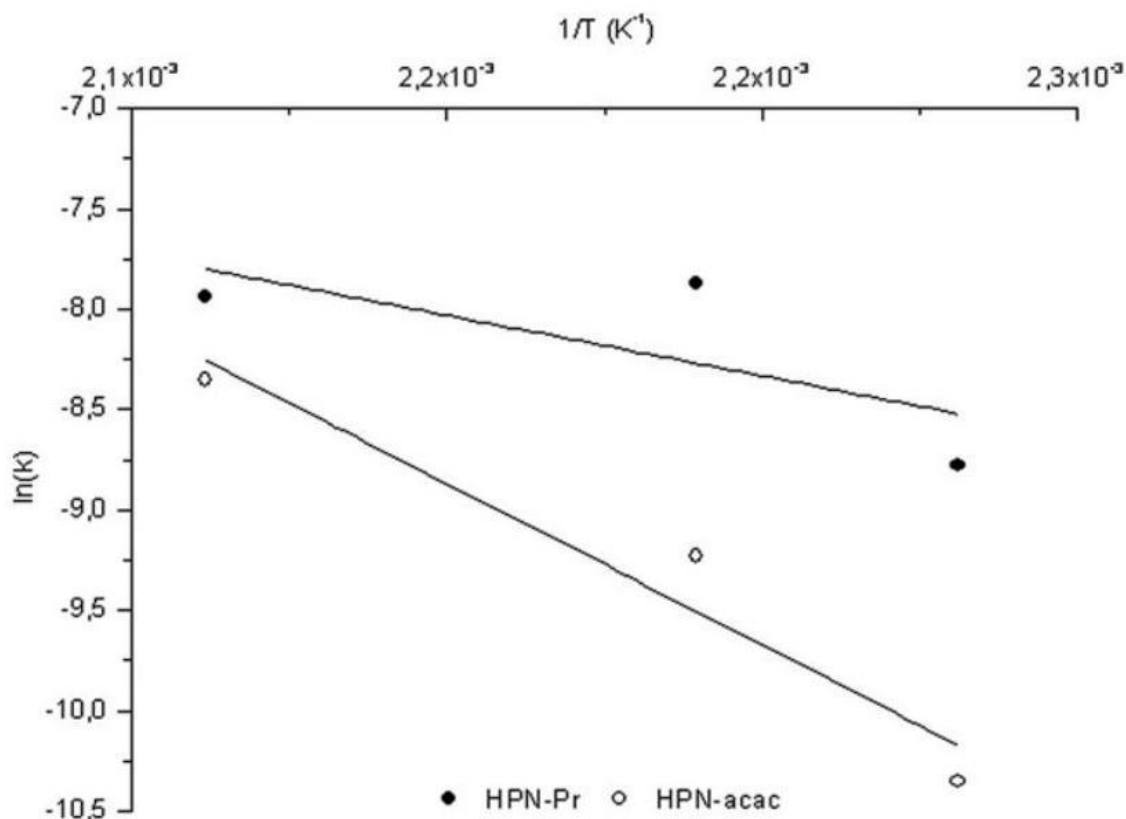


Fig. 8. - Arrhenius plots for the synthesis reactions of HPN-Pr and HPN-acac.

Table  
DSC results obtained for HPNs.

2

	$T_m$ (°C)	$\Delta H$ (J/g)	$X_c$ (%)
PP-g-MA	162.50	96.07	58.23
HPN-Pr	155.80	76.61	46.43
HPN-acac	161.36	60.02	36.32
HPN-acac hydrolysis 96 h	159.80	46.62	28.21

analysis (TGA) and of melting temperature and crystallinity degree (Table 2), determined by differential scanning calorimetry (DSC).

The TGA results presented in Fig. 7 show that HPN-Pr start to loose weight around 100°C due to evaporation of some residual reactions sub-products. During the synthesis of HPN-Pr, 2-propanol (C<sub>3</sub>H<sub>7</sub>OH) is formed as a sub-product. This alcohol has a boiling point of 82.5°C, which explains the first weight variation. Comparing the curves of PP-g-MA and HPN-Pr, it can be observed that the latter has higher thermal stability. This behaviour can be due to the crosslinking bonds between organic and inorganic components. The residual value obtained ( 0.8592 mg ) was a little higher than the one ( 0.6873 mg ) that was calculated assuming that only Al<sub>2</sub>O<sub>3</sub> species would be present at 550°C.

As expected, HPN-acac has a different thermal behaviour before and after hydrolysis. Before, it shows a first step decomposition around 190°C, which corresponds to the Al(acac)<sub>3</sub> melting temperature and then has a second one due to matrix degradation. After hydrolysis, degradation change for one-step process, indicating that all acac reacted during hydrolysis in agreement with FT-IR (Fig. 1). Comparing the degradation curves of HPN-acac with and without hydrolysis treatment it can be seen that the final degradation temperature is the same. Moreover, it is clear that the residual weight is higher for the sample before hydrolysis ( 2.10 before and 0.36wt. % after). This is in line with previous results that evidence that the amount of inorganic particles decreases after hydrolysis.

DSC data obtained for PP-g-MA and HPNs are presented in Table 2. The crystalline fraction ( $X_c$ ) was calculated from melting enthalpy, using Eq. (3).

$$X_c = \frac{\Delta H}{\Delta H^0} \times 100 \quad (3)$$

where  $\Delta H$  is the melting enthalpy of the material given by the area under the endothermic peak, and  $\Delta H \approx 165$  J/g is the melting enthalpy for 100% isotactic PP [22].

The crosslinking structure of HPN-Pr influences the crystalline regions of PP-g-MA matrix. In fact, the melting temperature, melting enthalpy and crystallinity degree of HPN-Pr is lower than the matrix. This is explained by the effect of crosslinking on crystallinity regions, which inhibits the folding of macromolecules chains and decrease the lamellar crystals. The formation of crosslinking between organic and inorganic components of HPN-Pr, during sol-gel reaction, disturbs the reorganization and chain folding during crystallization process, which results imperfect crystallites formation with smaller size and also less content. All this parameters contributed for the observed decrease in melting temperature, enthalpy and crystallinity degree for HPN-Pr [26].

In case of HPN-acac before and after hydrolysis, a decrease on melting enthalpy and crystallinity degree was observed. This decrease was driven by a reduction on structural regularity and separation of chains by the presence of organic group (acac), which obstructs or disturbs the reorganization and the folding of macromolecular chains, decreasing in general the size and content of the crystals. After hydrolysis this effect was even higher due to the formation of more crosslinking bonds, resulting in new decrease of crystallinity degree and melting temperature.

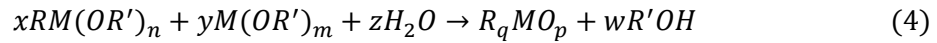
## General discussion

### Effect of the precursor organic groups size on the reaction

In order to explain better and understand the results obtained with each aluminium precursor used in the present work, the activation energy ( $E_a$ ) involved in the synthesis of the HPNs was determined. Fig. 8 depicts the Arrhenius plots obtained for HPN-Pr and HPN-acac. A linear relationship was found for the reactions with both precursors. The  $E_a$  was 52.9 kJ/mol and 113.9 kJ/mol for HPN-Pr and HPN-acac, respectively. According to the results shown above, the Al(acac)<sub>3</sub> precursor has a higher  $E_a$  value. This can be attributed to the volume of its organic groups ( $-O_2C_5H_7$ ), which may prevent the chemical reaction with the maleic anhydride group of the PP. Thus, to promote the reaction between Al(acac)<sub>3</sub> and PP-g-MA it is necessary to provide more energy to the system to overcome the effect of the stereochemical hindrance. Contrarily, since the Al(Pr - i - O)<sub>3</sub> has a linear

organic chain ( $^{-}OC_3H_7$ ), the reaction is easier with this precursor and the  $E_a$  is lower. Bahloul and co-workers obtained similar  $E_a$  value ( 66 kJ/mol ) using titanium *n*-butoxide for the synthesis of  $TiO_2$  nanoparticles in PP matrix by reactive extrusion [12].

These results are in agreement with theory, as the extent of the sol-gel reaction, when aluminium alkoxides are used as inorganic precursor, depends mainly on the steric hindrance of the alkoxide ligand [30]. This group is bonded to the metal by hydrolytically stable way. Metal with alkoxide ligands type  $-O-CH_2-R$ , where *R* is: *n* -  $C_4H_9$ ; *i* -  $C_4H_9$ ; *n* -  $C_5H_{11}$ , etc., has lower steric hindrance as a result of molecules symmetry. However, if the alkoxide groups has a OR as secondary or tertiary, the conversion of tetrahedral Al atoms to penta or octahedral coordination, results in the formation of less species, like dimers or trimers [31] and consequently lower reactivity. Schubert et al, outlined the general equation for hydrolysis-condensation reaction of metal alkoxides, Eq. (4). If the  $M(OR')$  group changes by other more hydrolytically stable, the degree of crosslinking during the sol-gel process decreases [32,33]. This explains the behaviour of the precursors used in the present work.



## Reaction mechanism

Metal alkoxides are widely used as inorganic precursors due to their great reactivity resulting from the lower electronegativity of the metal and its ability to exhibit several coordination states. When

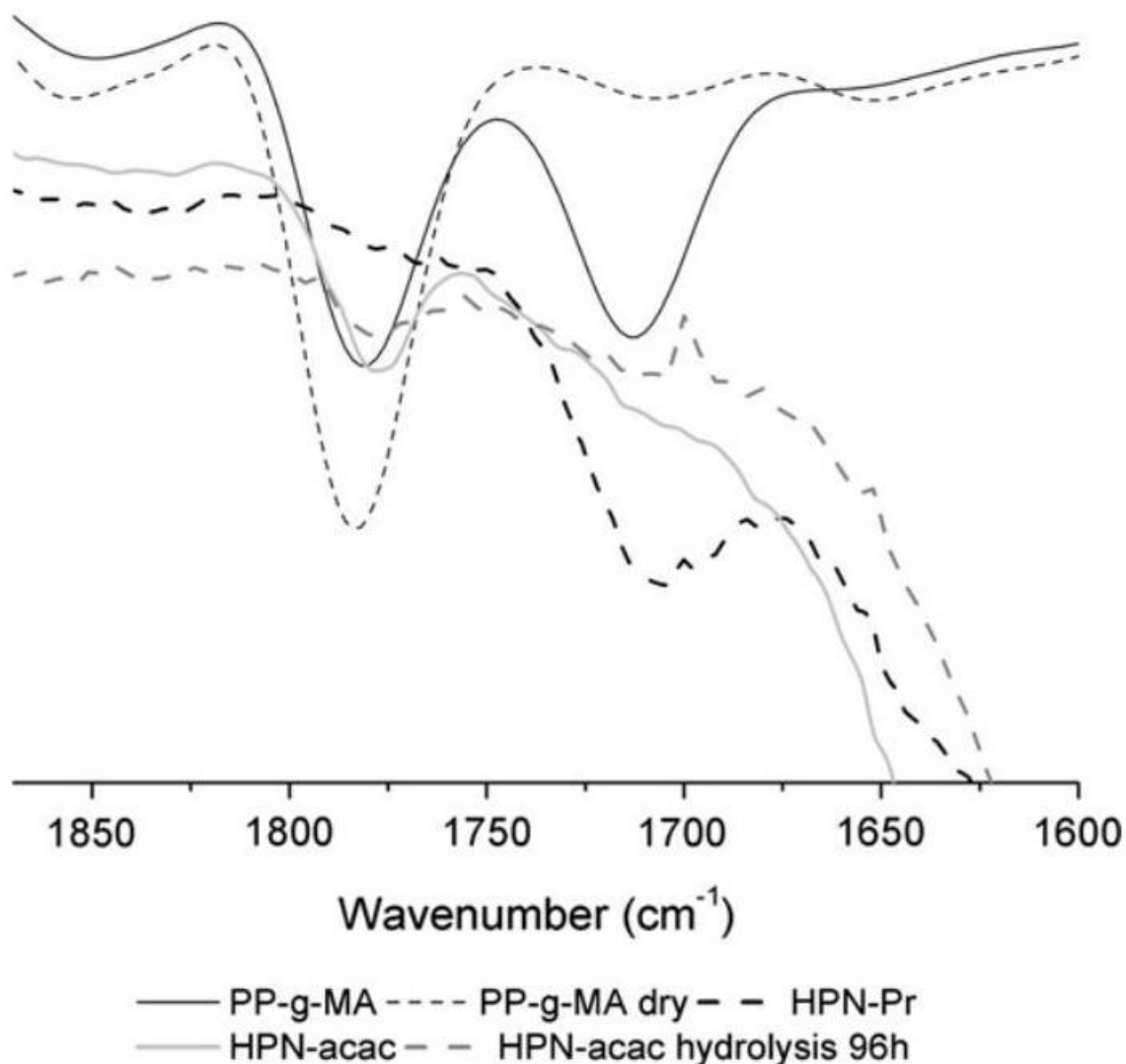


Fig. 9. - FT-IR of maleic anhydride ring for HPN-Pr and HPN-acac. the metal is in its saturated coordination state and in the absence of catalyst, the hydrolysis and condensation mechanism of the alkoxide occurs by nucleophilic substitution involving nucleophilic addition followed by a proton transfer from the attacking group to an alkoxide or hydroxo-ligand and the removal of the protonated species as, either, alcohol (alcoxolation) or water (oxolation) [30].

It is well known that during hydrolysis reaction, a decrease of anhydride absorbance at  $1780 \text{ cm}^{-1}$  and an increase of the carboxylic acid absorbance at  $1710 \text{ cm}^{-1}$  occur. The FT-IR results (Fig. 9) clearly show the ring open form of MA in the HPN-PR. Therefore, for the synthesis of HPN-Pr hydrolysis treatment was not necessary, the open form of the MA group was provoked by the formation of covalent bond between aluminium and PP-g-MA backbone. In case of HPN-acac, the close form of MA ring still predominant both before and after hydrolysis. This seems to indicated the absence or lower level of reaction between  $\text{Al}(\text{acac})_3$  precursor and MA groups of the PP-g-MA. Nevertheless, a decrease on acetylacetonate (acac) group bands at  $1520 \text{ cm}^{-1}$  and  $1580 \text{ cm}^{-1}$  together with the appearance of Al – OH stretching mode can be observed, as depicted in FT-IR results.

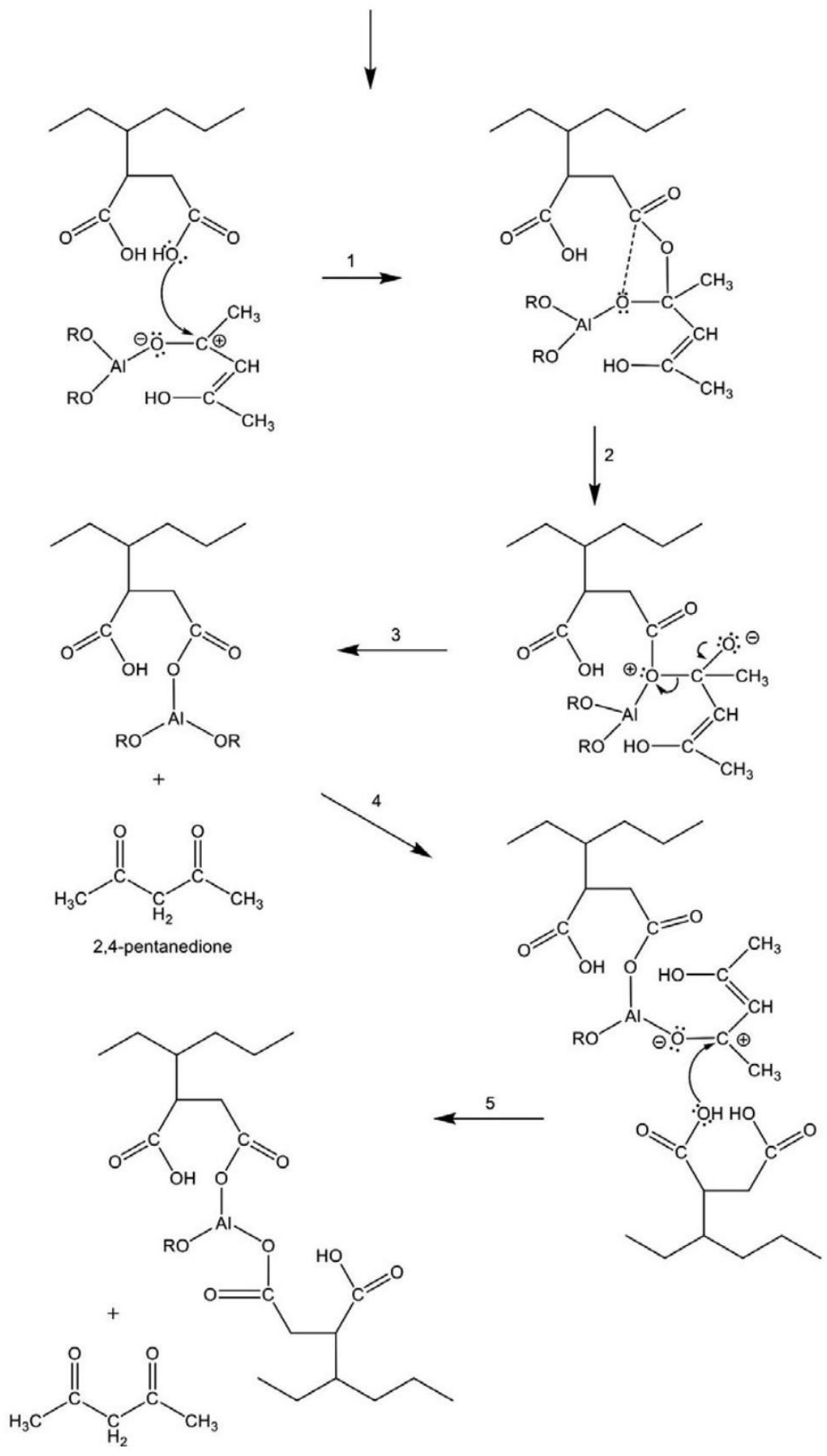
Taking this data into consideration and all the results obtained by the several techniques used, a reaction mechanism for each precursor is proposed in Fig. 10a and b.

The crosslinking structure obtained during HPN-Pr synthesis occurs by nucleophilic attack of oxygen bonded to aluminium to the carboxylic acid formed when the acid form of maleic anhydride is present (reaction 1). After nucleophilic attack the hydroxyl group of carboxylic acid comes out, reacting with organic group of aluminium isopropoxide ( $C_3H_7$ ), resulting in the formation of 2-propanol ( $C_3H_7OH$ ) and polymeric species containing aluminium (reaction 2). Then the crosslinking proceeds by the reaction between the polymeric specie formed in the previous step with another maleic anhydride group (reactions 3 and 4).

In the case of HPN-acac synthesis, the carboxylic group from the maleic anhydride reacts with aluminium acetylacetonate as describe in first reaction of Fig. 10b. In this case, due to the mesomeric form of the acetylacetonate group, the oxygen of hydroxyl group attacks the carbon of the precursor (reaction 1) [34]. In the second step, the carbocation suffers a rearrangement due to the interaction between the oxygen atom that has free electron pairs and the cationic centre of the carbon atom (reaction 2). Since the species formed is unstable, further rearrangement occurs resulting in PP containing aluminium and 2,4-pentanedione formation (reaction 3). After, the reaction continues between the previous polymeric formed specie and a new PP-g-MA molecule (reaction 4) forming crosslinking (reaction 5).

c.

Fig. 10. - Reaction mechanism of a) HPN-Pr and b) HPN-acac.  
 R= CHCH<sub>3</sub> CHCCH<sub>3</sub>O  
 OHHO



## Conclusion

This study confirms that it is possible to produce inorganic nanoparticles in a polymeric matrix by reaction in the molten state without solvents. Whereas the chemical reaction occurred in only one step process for  $\text{Al}(\text{Pr} - \text{i} - \text{O})_3$ , for  $\text{Al}(\text{acac})_3$  a post step treatment by hydrolysis was necessary. FT-IR spectroscopy, rheology, TGA, DSC analysis and gel content determination proved that aluminium formed covalent bonds with PP-g-MA. Thermal behaviour was also enhanced comparing with PP-g-MA, where the degradation temperature increased, being the onset around 450°C.

The reactions extend and the amount of aluminium depends on the precursor used. This was explained by the determination of the activation energy, which showed a lower value when precursor  $\text{Al}(\text{Pr} - \text{i} - \text{O})_3$  was used.

Taking into account all the results obtained, the reaction mechanisms for both precursor were proposed.

## Acknowledgment

The authors acknowledge the Foundation for Science and Technology (FCT) Project SFRH/BD/39085/2007 for the financial support.

## References

- [1] N.Y. Turova, E.P. Turevskaya, V.G. Kessles, M.I. Yanovskaya, *The Chemistry of Metal Alkoxides*, Kluwer Academic Publisher Ed., 2002.
- [2] Q. Dou, X. Zhu, K. Peter, D.E. Demco, M. Möller, C. Melian, *J. Sol-Gel Sci. Technol.* 48 (1-2) (2008) 51-60.
- [3] K.H. Wang, M.H. Choi, C.M. Koo, Y.S. Choi, I.J. Chung, *Polymer* 42 (24) (2001) 9819-9826.
- [4] L.J. Taylor, US Patent (1975) 3891594.
- [5] P. Judeinstein, C. Sanchez, *J. Mater. Chem.* 6 (4) (1996) 511-525.
- [6] C. Xu, K. Ohno, V. Ladmiral, R. Composto, *Polymer* 49 (16) (2008) 3568-3577.
- [7] M.Z. Rong, M.Q. Zhang, Y.X. Zheng, H.M. Zeng, R. Walter, K. Frieddrich, *Polymer* 42 (1) (2001) 167-183.
- [8] X. Liua, Q. Wu, *Polymer* 42 (25) (2001) 10013-10019.
- [9] French Patent Dow Corning n8 69.43.985, 1968.
- [10] M.Z. Rong, M.Q. Zhang, S.L. Pan, K. Friedrich, *J. Appl. Polym. Sci.* 92 (3) (2003) 1771-1781.
- [11] J. Krueenate, R. Tongpool, T. Panyathanmaporn, P. Kongrat, *Surf. Interface Anal.* 36 (8) (2004) 1044-1047.
- [12] W. Bahloul, O. Oddes, V. Bounor-Legaré, F. Mélis, P. Cassagnau, B. Vergnes, *Am. Inst. Chem. Eng.* 57 (8) (2011) 2174-2184.
- [13] S. Jain, H. Goossensa, M. van Duinb, P. Lemstra, *Polymer* 46 (20) (2005) 8805-8818.
- [14] S. Jain, H. Goossensa, F. Picchionia, P. Magusinb, B. Mezarib, M. van Duin, *Polymer* 46 (17) (2005) 6666-6681.
- [15] H. Zou, S. Wu, J. Shen, *J. Chem. Rev.* 108 (9) (2008) 3893-3957.

- [16] D. Sun, R. Zhang, Z. Liu, Y. Huang, Y. Wang, J. He, B. Han, G. Yang, *Macromolecules* 38 (13) (2005) 5617-5624.
- [17] W. Bahloul, V. Bounor-Legaré, L. David, P. Cassagnau, *Physics* 48 (11) (2011) 1213-1222.
- [18] Y. Shieh, J. Liau, T. Chen, *J. Appl. Polym. Sci.* 81 (1) (2001) 186-196.
- [19] I.H. Joe, A.K. Vasudevan, G. Aruldas, A.D. Damodaran, K.G.K. Warriar, *J. Solid State Chem.* 131 (1) (1997) 181-184.
- [20] J.H. Wengrovius, M.F. Garbaskas, E.A. Williams, R.C. Going, P.E. Donahue, J.F. Smith, *J. Am. Chem. Soc.* 108 (5) (1986) 982-989.
- [21] Z. Stojanovic, Z. Kacarevic-Popovic, S. Galovic, D. Milicevic, E. Suljovrujic, *Polym. Degrad. Stabil.* 87 (2) (2005) 279-286.
- [22] S. Sakka, *Handbook of Sol-gel Science and Technology: Processing Characterization and Applications. Volume III: Applications of sol-gel Technology*, Kluwer Academic Publishers Ed., 2004.
- [23] A. Tonejc, M. Stubičar, A.M. Tonejc, K. Kusanović, B. Subotić, I. Smit, *J. Mater. Sci. Lett.* 13 (1994) 519-520.
- [24] D. Mishra, S. Anand, R.K. Panda, R.P. Das, *Mater. Lett.* 42 (1-2) (2000) 38-45.
- [25] K.M.S. Khalil, *Appl. Surf. Sci.* 255 (5Part 2) (2008) 2874-2878.
- [26] C. Wu, *J. Appl. Polym. Sci.* 92 (3) (2004) 1749-1757.
- [27] C. Yang, J. Kim, J. Choi, M. Kwon, Y. Kim, J. Choi, G. Kim, *J. Ind. Eng. Chem.* 6 (3) (2000) 149-156.
- [28] H.A. Khonakdara, J. Morshediana, U. Wagenknechtb, S.H. Jafari, *Polymer* 44 (15) (2003) 4301-4309.
- [29] J. Brand, W.G. Sloof, H. Terryn, J.H.W. Wit, *Surf. Interface Anal.* 36 (1) (2004) 81-88.
- [30] C.J. Brinker, G.W. Scherer, *Sol-gel Science - The Physics and Chemistry of SolGel Processing*, Academic Press Ed., 1989.
- [31] V. Maneeratana, *Alkoxide-based precursor for direct electrospinning of aluminum fibers*. PhD Thesis, 2007, pp. 49-52.
- [32] J.H. Wengrovius, M.F. Carbauskas, E.A. Williams, R.C. Going, P.E. Donahue, J.F. Smith, *J. Am. Chem. Soc.* 108 (108) (1986) 982-989.
- [33] U. Schubert, N. Husing, A. Lorenz, *Chem. Mater.* 7 (11) (1995) 2010-2027.
- [34] Z. Czech, M. Wojciechowicz, *Eur. Polym. J.* 42 (9) (2006) 2153-2160.

---

E-mail addresses: [moliveira@dep.uminho.pt](mailto:moliveira@dep.uminho.pt) (M. Oliveira), [avm@dep.uminho.pt](mailto:avm@dep.uminho.pt) (A.V. Machado).